Ionic structure, Liquid-liquid phase transitions, X-Ray diffraction, and X-Ray Thomson scattering in shock compressed liquid Silicon in the 100-200 GPa regime.

M.W.C. Dharma-wardana,[1, 2, *] Dennis D. Klug,[1, †] Hannah Poole,[3, ‡] and G.Gregori[3, §]

[1] *National Research Council of Canada, Ottawa, Ontario. Canada K1A 0R6*
[2] *Département de Physique, Université de Montréal, Montréal, Québec, Canada H3C 3J7*
[3] *Department of Physics, University of Oxford, Oxford OX1 3PU, United Kingdom*

Recent cutting-edge experiments have provided *in situ* structure characterization and measurements of the pressure (P), density ($\bar{\rho}$) and temperature (T) of shock compressed silicon in the 100 GPa range of pressures and up to ∼10,000K. We present first-principles calculations in this $P, T, \bar{\rho}$ regime to reveal a plethora of novel liquid-liquid phase transitions (LPTs) identifiable via discontinuities in the pressure and the compressibility. Evidence for the presence of a highly-correlated liquid (CL) phase, as well as a normal-liquid (NL) phase at the LPTs is presented by a detailed study of one LPT. The LPTs make the interpretation of these experiments more challenging. The LPTs preserve the short-ranged ionic structure of the fluid by collective adjustments of many distant atoms when subject to compression and heating, with minimal change in the ion-ion pair-distribution functions, and in transport properties such as the electrical and thermal conductivities σ and κ. We match the experimental X-Ray Thomson scattering and X-ray diffraction data theoretically, and provide pressure isotherms, ionization data and compressibilities that support the above picture of liquid silicon as a highly complex LPT-driven "glassy" metallic liquid. These novel results are relevant to materials research, studies of planetary interiors, high-energy-density physics, and in laser-fusion studies.

PACS numbers: 52.25.Jm,52.70.La,71.15.Mb,52.27.Gr

I. INTRODUCTION

Laboratory-based study of extreme states of matter, as found in planetary interiors, or matter produced in high-energy laser-matter interactions etc., depends crucially on the development of simultaneous-measurement facilities coupled to advanced instruments, e.g., such as the Linac Coherent Light Source and the the OMEGA-EP laser facility [1]. The characterization of these states of matter, usually named "warm-dense matter" (WDM) [2, 3], by simultaneously measuring their pressure (P), temperature (T), and density ($\bar{\rho}$), as well as the ionic and electronic structure is a necessary step for testing the applicability of available theories of WDM. These theories, crucial even to nuclear-stockpile stewardship programs, are the only means of going beyond the reach of laboratory-based studies which are limited by the energy scales of terrestrial facilities.

Si, together with C, P, As etc., are light elements that are insulators or semiconductors that become metallic liquids when molten, with an increase in density. They manifest transient covalent binding even after melting [4–8]. Furthermore, Si is of fundamental importance in the physics of planetary interiors, and in many areas of materials science, device fabrication and shock physics [9]. The electrical and thermal conductivities of l-silicon are also of interest in the context of planetary magnetism and thermal balance.

It's fundamental physics is also intriguing and challenging due to the presence of many liquid-liquid phase transitions (LPTs) [10, 11]. The LPTs are also known as plasma-phase transitions. The LPTs in liquid-Si include a well-studied transition between a high-density branch of the liquid and the low-density branch at a density of ∼2.27-2.5 g/cm^3 at ∼1200-1800K, near its melting point. A highly-correlated phase appears near the LPT and persists even into the supercooled regime (1200K) [11–22]. We refer to this LPT as LPT(2.5|1200K) in the foregoing. The persistence of these LPTs even to temperatures as high as 1 eV (11,604K) was predicted in Ref. [10] but experimental studies of such WDM states have been lacking.

The recent study of shock-compressed liquid silicon (l-Si) by Poole et al [1] in the 100 GPa regime has provided simultaneously measured data for X-Ray Thomson scattering (XRTS) and X-Ray diffraction (XRD), as well as pressure and temperature determinations. They conclude that the WDM-Si created was at a density of 4.56±0.07 g/cm^3, with a pressure of 106±6 GPa. However, these estimates need to be re-examined using a first-principles atomic physics model.

A first-principles approach to the analysis of such data is to use N-atom DFT calculations, coupled to molecular dynamics (MD) simulations [23, 24], a method referred to here as 'quantum molecular dynamics' (QMD). It is also sometimes referred to as MD-DFT in the literature. Poole et al [1] did not use QMD, pointing out that "such methodologies [25, 26] are computationally expensive and introduce varying degrees of complexity". Their study was conceived more as a proof-of-principle

* Email address: chandre.dharma-wardana@nrc-cnrc.gc.ca
† Email address: ddklugca@gamil.com
‡ Email address: hannah.poole@rochester.edu
§ Email address: gianluca.gregorie@physics.ox.ac.uk

application of a multi-messenger diagnostic approach. As such, to maintain fast computations within a Markov-Chain Monte Carlo analysis, they opted for a simple pair-potential model [27] that uses a non-linear Hulthén (NLH) potential. They analyzed the XRD and XRTS data, with the pressure estimated from an equation of state (EOS) model due to Vorberger et al [28], and Ebeling et al [29]. They concluded using only velocity interferometry measurements (VISAR) that the l-Si had a density of 4.43± 0.8 g/cm^3, revised using XRD data to ∼4.6 g/cm^3, with T =5300K, and a charge state with $\bar{Z} = 1.3$, i.e., each 'average' Si atom has given up 1.3 electrons to become $Si^{1.3+}$ ions.

In QMD, many silicon atoms, e.g., $N = 64 - 216$ or more are used to capture many-ion (Si-Si) interactions, while an electron XC-functional reduces the many-electron problem to an effective "non-interacting", i.e., "single-electron" model as in a Lorentz plasma [30] where only electron-ion interactions need to be dealt with. In the same way, the N-ion problem can be reduced to an effective "one-ion" problem by using an XC-functional suitable for ion-ion interactions [31]. The XC-functionals used in the NPA are discussed in more detail in the appendix. It is this effective "one-ion" DFT approach, known as the neutral-pseudo-atom (NPA) approach [31–34] that we use in our calculations. A recent account of the NPA method may be found in Ref. [10]. It is similar to an average-atom (AA) model and hence computationally very economical, unlike QMD. We also ascertain, using limited QMD calculations, that the structure data obtained from the NPA and from the QMD are in good agreement.

Using the NPA technique we calculate the structure factors, pair-distribution functions (PDFs), pressure isotherms, comprehensibility electrical and thermal conductivities σ, κ for l-Si for densities within 4.0 g/cm^3-5.0 g/cm^3. The main peaks of the calculated structure factors $S_{ii}(k)$ are found to be nearly self-similar and located very nearly at $k_1 = 1.5k_F$, where k_F is the Fermi wave vector. As discussed in the Appendix, the main peak of $S(k)$ gets positioned to take advantage of the zero of the electron-ion pseudopotential $U_{ei}(k)$. The interaction potentials are very long-ranged due to Friedel tails. Hence all charge distributions are calculated to about ten Wigner-Seitz radii or more. When the fluid is compressed or heated, small collective displacements of many distant ions occur to preserve the short-ranged ordering, by inducing many LPTs and discontinuities in the compressibility and the pressure.

These LPTs have only a minimal impact on the conductivites σ, κ. This arises since the main peak of $S_{ii}(k)$, and the window of interaction of the electron-ion pseudopotential around $2k_F$, remain largely unaffected in the range of small $t = T/E_F$, where E_F is the Fermi energy. Thus, for $\bar{\rho}$ =4.6 g/cm^3, $T = 1$ eV, $t = 0.051$.

It is hard to detect LPTs using QMD simulations (unless they directly affect short-ranged ordering) because, even in a simulation using 216 atoms; the linear scale is about 6 Wigner-Seitz radii. The central atom has no more than two to three neighbours on each side. The interionic potentials generated in such QMD simulations are thus very short ranged, compared to those from NPA calculations, as was demonstrated in Ref. [35], for the pair-potentials for carbon extracted from QMD calculations of Whitley et al [36]. Machine-learnt potentials [37–39] using multi-ion models (e.g., extensions of the Stillinger-Weber model or effective-medium models), bond-order potentials etc., have not been successful in their applications to these WDM systems [35, 40]. A similar problem arises in the study of Martensitic transitions in iron [42] where small collective modifications in positions of many 'far-away' ions interacting via long-ranged potentials occur. In contrast, if significant changes in short-range order occur at an LPT, then QMD calculations with even 64 atoms using the PBE functional may be sufficient. However simulations with 216 atoms and the SCAN functional are recommended in Remsing et al. [21], for instance, to obtain quantitative predictions of the melt line of silicon.

Besides the LPTs that preserve the short-ranged order, there are also correlated liquid phases that appear between the high-density branch and the low-density branch that form an LPT. Here even supercooled persistent states, identified as somewhat solid-like correlated liquid (CL) phases have been revealed in dynamic simulations [22], as in the LPT at 2.5 g/cm^3 near the melting point of Si.

In this study, directed more to a reinterpretation of the XRTS and XRD data, a full analysis of the LPTs will not be attempted. Instead, we will study just one of them in some detail, to report the observation of a correlated liquid state and to bring out the similarities to the well-studied LPT(2.5|1200K) of normal-density Si near its melting point [10].

The presence of LPTs in l-Si renders it highly viscous, prone to hysteresis, and "glassy" to shock propagation, slowing down shock speeds. This may lead to lower estimates of pressure and temperature for shocked media if the LPTs are ignored. Our calculations simulate the XRD and XRTS data of Poole et al [1] and show that their estimate of T=0.4567 eV (5300K) and a pressure of 100 GPa, with $\bar{Z}$=1.3 are indeed lower estimates compared to ours. We find $T \sim$ 1-1.2 eV, $P \sim$ 150 GPa, and $\bar{Z}$=4.

We present first-principles pressure (P), compressibility (ξ), transport (σ, κ), and ionic structure data, as well as XRTS and XRD intensity spectra. The notation for ion-ion data will be simplified in the foregoing to, e.g., $S(k) = S_{ii}(k), g(r) = g_{ii}(k)$ when no confusion is likely to arise. The theoretical results show good agreement with the available experimental data and QMD simulations of structure data. Additional details of these calculations are given in the Appendix.

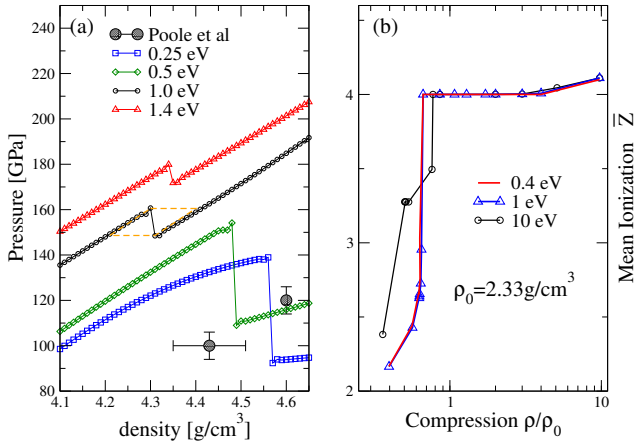

FIG. 1. (online color) EOS data implying large hysteresis in compression/expansion, and in heating/cooling processes in l-Si. (a) Pressure isotherms in the density range 4.1-4.7 g/cm^3 display many discontinuities due to liquid-liquid phase transitions [10] The data point derived from the experiment, Ref. [1], using their atomic model and only VISAR measurements (4.43 g/cm^3), and the data point for final density of 4.6 g/cm^3 based on VISAR, XRD and XRTS are also shown. (b)The mean ionization $\bar{Z}$ as a function of compression $\bar{\rho}/\rho_0$, where ρ_0=2.33 g/cm^3.

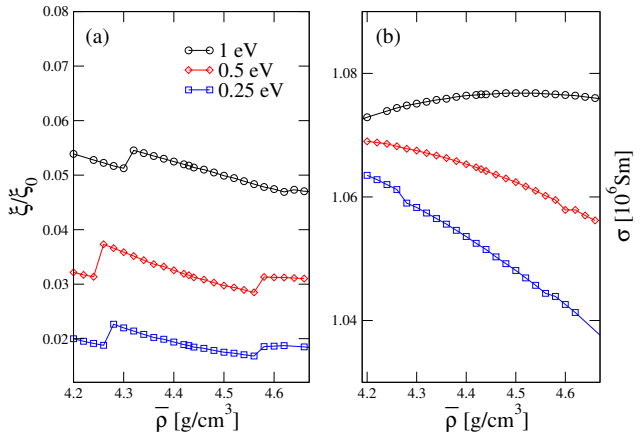

FIG. 2. (online color) (a) Discontinuities in $S(0) = \xi/\xi_0$, the compressibility ratio, independently confirms the LPTs. (b) The electrical conductivity σ is only very weakly affected by the LPTs. At $T = 025$ eV, σ changes by less than 3% when the density changes by about 25%. At $T = 1$ eV the change is only a fraction of a percent (c.f., Appendix).

II. STRUCTURE DATA AND EOS

We use Hartree atomic units $\hbar = |e| = m_e = 1$ in a standard notation. The electron-sphere radius $r_s = [3/(4\pi\bar{n})]^{1/3}$, the ion Wigner-Seitz radius $r_{ws} = \bar{Z}^{1/3} r_s$, and the Fermi wavevector $k_F = (2\pi^2\bar{n})^{1/3}$ are used in our equations and graphics.

As discussed in more detail in the Appendix, the NPA provides electron-ion pseudopotentials $U_{ei}(k)$, pair potentials $V_{ii}(r)$, pair-distribution functions (PDFs) $g(r)$, the structure factor $S(k)$. It provides all electronic-structure data necessary for the calculation of the total Helmholtz free energy of the system as well as all other properties including XRTS data and transport properties, from first principles.

The isothermal compressibility ξ of the fluid is directly available from the $k \to 0$ limit of $S(k)$, viz., $S(0) = \xi/\xi_0$, where $\xi_0 = 1/(\bar{\rho}T)$ is the ideal-gas compressibility. Discontinuities in the pressure and the $S(0)$ reveal the presence of a plethora of liquid-liquid phase transitions. Unlike in QMD where the small-k limit of $S(k)$ is not accessible due to the finite size of the simulation cell, the large radius of the correlation sphere used in the NPA enables an accurate evaluation of the $S(0)$ limit.

Fig. 1 provide EOS data for l-Si indicating abrupt breaks due to LPTs similar to the well-know transition near ∼2.2-2.5 g/cm^3 at the melting line [10, 21]. The figure also shows how the experimental data point (see Table III [1]) evolves when only VISAR data are used in the analysis, and when a more complete set of diagnostics (XRD, XRTS) is used in the analysis.

In Fig. 2(a) we display the compressibility ratio ξ/ξ_0 of l-Si, confirming the LPTs observed in the P-isotherms. Usually, phase transitions also imply abrupt changes in the electrical and thermal conductivities if changes occur at the Fermi surface. What is noteworthy here is that while the density changes from $\sim$ 4 g/cm^3 to $\sim$ 5 g/cm^3, i.e., a change of 25%, the electrical conductivity changes less than 3% at $T = 0.25$ eV, while at 1 eV, the change is less than 0.3%. The same is true for the thermal conductivity given in table II of the appendix. Furthermore, as seen in Fig. 2(b), the LPTs have very little impact on these transport properties. This is well accounted by our theoretical results which show that (i) the mean ionization $\bar{Z}$ remains unchanged across these LPTs; (ii) any significant variation in the position of the first peak of $S(k)$ is suppressed as it remains tied to a zero of the form factor of the pseudopotential, thereby reducing the electron-ion interaction energy at the Fermi surface. (iii) Although a $g(r)$ of a highly-correlated liquid (CL) is detected near LPTs through simulations, it seems to have no impact on the conductivity [10].

Our analysis of the XRTS and XRD data favour a density of $\sim$ 4.3 to 4.4 g/cm^3,T=1 to 1.2 eV, at a pressure of $\sim$ 150 GPa. This higher P, T compared to the estimate of Ref. [1] is consistent with an extremely glassy material, caused by the LPTs. Furthermore, panel (b) of Fig. 1 show that a value of $\bar{Z} = 1.3$ as in Ref. [1] is not attained even at the lowest density of 0.93 g/cm^3, compression $\sim$ 0.4 for temperatures of 0.4 eV to 10 eV. We have confirmed this even at 0.25 eV, though not displayed in Fig. 1. Furthermore, it was shown [10] that the Ganesh-Widom pressure data [18] along the melt line of l-Si at 2.33 g/cm^3 is recovered in NPA calculations with $\bar{Z} = 4$ as the mean ionization. We also find that the NHL potential is unable to generate the known structure data (e.g., $g(r)$) for l-Si at, e.g., 2.5 g/cm^3 and $T = 1800$K, at the Si-melt line.

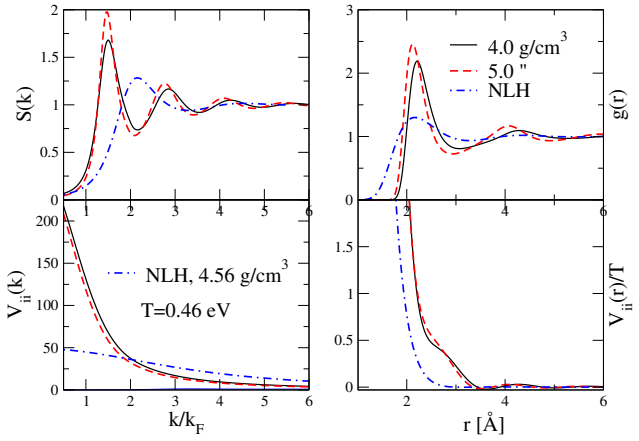

FIG. 3. (online color) Panel (a) The structure factor for l-Si at 4.0 g/cm^3, and at 5.0 g/cm^3 at T=0.4567 eV obtained from the NPA approach, compared with the $S(k)$ used in Ref. [1] derived from the NLH potential at 4.56 g/cm^3 at T=0.46 eV. The k-axis is scaled with the appropriate k_F. (b) Comparison of the PDFs $g(r)$. (c) Comparison of the pair-potentials in k-space. (d) The real-space potentials $V_{ii}(r)$.

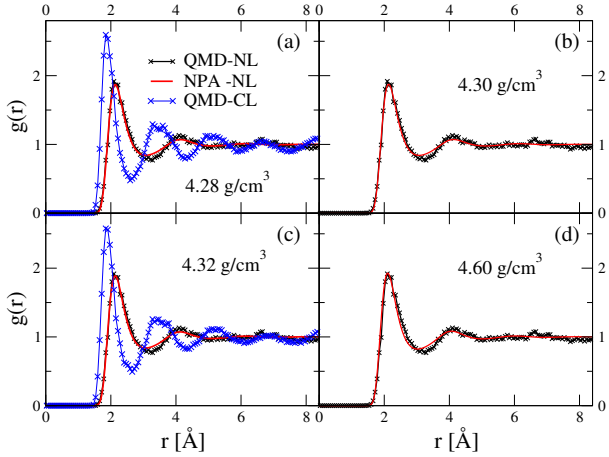

FIG. 4. (online color) The PDFs $g(r)$ obtained via NPA and from QMD-VASP at densities near the LPT at 4.3 g/cm^3 and $T = 1$ eV. The NPA and VASP-QMD generated $g(r)$ agree closely for the normal-liquid (NL) phase. A highly-correlated liquid (CL), with the 1st peak in $g(r)$ closer in (< 2Å), and is found and displayed in panels (a) and (c). This was not detected at the higher density of 4.6 g/cm^3, away from the LPT, where only the normal liquid is found.

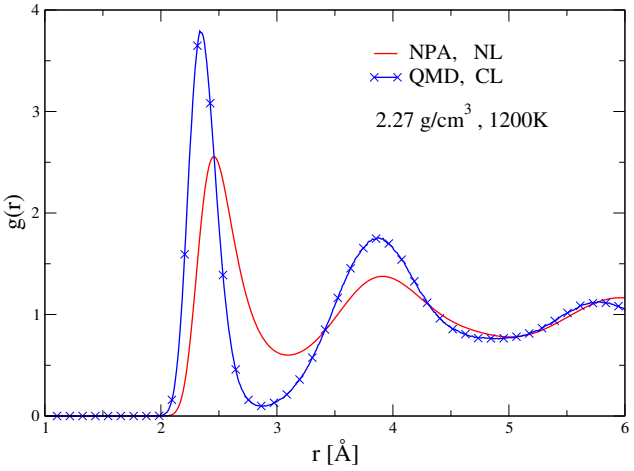

FIG. 5. (online color) The PDFs $g(r)$ obtained via NPA and from QMD (216 atoms+SCAN functional [21, 22]) at densities near the LPT at 2.27 g/cm^3 and $T = 1200$K. The NPA and QMD generated $g(r)$ agree closely for the normal-liquid phase. The highly-correlated liquid (CL) similar to those in Fig. 4(c),(d), with the 1st peak in $g(r)$ closer-in than the usual Si-Si bond distance of 2.35 Å, has been reported in [10, 22].

The comparison of the potentials and structure data shown in Fig. 3 shows that there is a large difference between the NPA results and the NLH model. The latter is closely similar to the Yukawa model and hence this lack of agreement with a first-principles atomic model is not unexpected.

Furthermore, we show below that the XRTS ad XRD profiles are in much better agreement with the NPA calculation. The $S(k)$ and $g(r)$ calculated for various WDM conditions using the NPA method has been shown to agree very closely with those obtained by QMD simulations in all instances where comparisons are available, and more specifically for l-Si [10, 43] as well. As the current study is concerned with compressed Si in the regime of density $\bar{\rho}$ 4.3-4.6 g/cm^3 and T in the range 0.46 eV to 1.2 eV, specific comparisons of the pair-distribution functions $g(r)$ obtained using the NPA, and QMD calculations using the Vienna Ab-initio Simulation code (VASP) were carried out, and examples are given in the following section where we discuss in detail the LPT at 4.3 g/cm^3 and $T = 1$ eV.

III. THE LPT AT 4.3 g/cm^3 AND 1 eV

Fig. 1 reveals six LPTs on the three isotherms shown there. A comprehensive study of all the LPTs, as was done for LPT(2.5|1200K) [10] making extensive use of QMD, is computationally costly and beyond the scope of this work. Instead, we study just the prominent LPT near $\bar{\rho} = 4.3$ g/cm^3 and $T = 1$ eV, viz., LPT(4.3|1eV) as this is closest to the density and temperature revealed by our study of the XRTS data discussed in Sec. IV.

We note that the short-ranged structures of the LPTs at 1 eV as revealed by the $g(r)$ calculated via the NPA for the stable liquid phase remain essentially unchanged across the LPTs and even for the full range of $\bar{\rho}$/gcm^{-3} from 4.28 to 4.6, as seen in Fig. 4. The NPA $g(r)$ and the $g(r)$ calculated via the VASP code agree very well for the normal form of l-Si. Details of VASP calculations are given in the Appendix. A more correlated liquid phase is also detected at $\bar{\rho}$/gcm$^{-3} = 4.28$ and 4.32. At first sight it is surprising that such a correlated phase might exist

at as high a temperature as 1 eV. However, $T = 1$ eV is only $T/E_F = 0.053$ at this compression.

As with the LPT(2.5|1200K), the CL-phase is difficult to obtain via the NPA which seeks the lowest-energy uniform-fluid phase. Whether this correlated phase plays a role in hysteresis loops, and even under supercooling, as was found for the LPT(2.5|1200K) using the SCAN functional and QMD calculations, have not been investigated in this work. However, we conclude from this limited study that the LPTs found here are similar to the LPT(2.5|1200K) studied in Ref. [10] for l-Si. Further discussions of the $g(r)$ and $S(k)$ of l-Si at the LPTs are given in Sec. A 4.

IV. X-RAY DIFFRACTION AND X-RAY THOMSON SCATTERING PROFILES

The NPA model has been successfully used already for analyzing XRTS and XRD data [44]. The Kohn-Sham calculation of the NPA provides the Fourier transform of the bound, and free electron density, viz., $n_b(q)$, $n_f(q)$ respectively. The 'ion feature' $I_{coh}(k)$ which is proportional to the scattered signal is such that $I_{coh}(k) = |n_b(k) + n_f(k)|^2 S(k)$. The observed signal includes an incoherent scattering signal $I_{inc}(k)$ as well. The scaled scattering signal provided by the experiment of Ref. [1] and the results from the NLH model are shown in Fig. 3(a) of Poole et al. We simulate their experimental data (Fig. 6) using the NPA-calculated ion-feature $W(k)$, to which $I_{incoh}(k)$ has been added, following Ref. [1].

The experimental signal I_{lqd} has been scaled to match the very high-k limit of a calculated value of I_{ic}

$$I_{lqd}/\gamma = I_{coh}\{S(k) - 1\} + I_{ic} \quad (1)$$

$$I_{ic} = I_{coh}(k) + I_{incoh}(k) \quad (2)$$

V. DISCUSSION

While the NPA-calculated XRD profile matches the experimental XRD data closely, the intensity is overestimated by $\sim 6\%$. A better fit can be obtained by slightly increasing the temperature of the fluid. However, given the error bars of the experiment, and the strong likelihood of hysteresis in this system, further optimization of the fit adds little insight. In our view, the higher estimate of $P \sim 150$ GPa, $T \sim 1.2$ eV, $\bar{\rho} = 4.35$ g/cm^3 obtained here, compared to $P \sim 100$ GPa, $T = 0.46$ eV is consistent with l-Si being a glassy LPT-ridden liquid rather than a simple liquid, as assumed in currently available Si-Hugoniots.

The existence of transient covalent bonds in liquid metals and plasmas such as l-carbon, l-Si and other low-Z materials has been appreciated by many workers since the 1980s. A description of such bonding states in terms of Wannier functions [45] may be possible and might be appropriate near the percolation threshold that would occur as $\bar{Z}$ decreases with decreasing density, as shown in Fig. 1(b). A Wannier-function description may also be appropriate for modeling the more-ordered CL-phase found at LPT(4.3|1 eV) and at the LPT(2.5|1200K). However, the normal-liquid phase is the most persistent form of l-Si. The normal liquid $S(k)$ has been used here, in the interpretation of the X-ray scattering data. Given that the WDM-Si studied here is in the strongly metallic regime with $\bar{Z} = 4$, the Kohn-Sham states of the continuum electrons are well represented by phase-shifted plane waves. This is attested by the fact that a simple weak s-wave pseudopotential (constructed *in situ* from the displaced Kohn-Sham density) is sufficient to describe ion-ion interactions.

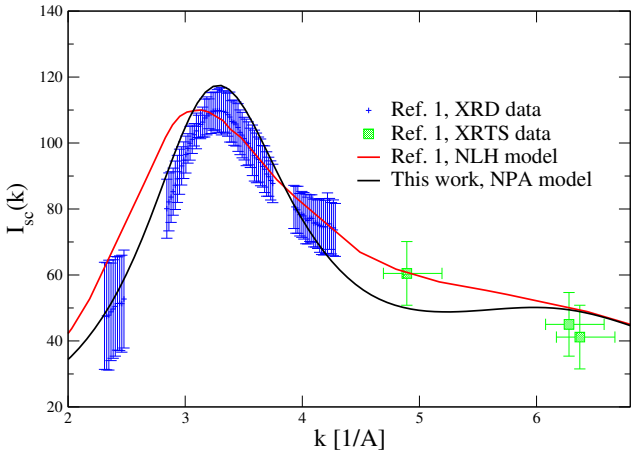

FIG. 6. (online color) The calculated scattered-light intensity is compared with the experimental X-ray diffraction (XRD) data and X-ray Thomson scattering (XRTS) data. The results for the NLH potential is from Ref. [1] with $\bar{\rho}$=4.6 g/cm^3, $\bar{Z}$ = 1.3, and T = 0.4567 eV. The NPA calculation is at $\bar{\rho}$=4.35 g/cm^3, $\bar{Z} = 4.0$, and T=1.2 eV.

Furthermore, the low ionization of $\bar{Z} \simeq 1.3$ proposed in Ref. [1] is a result of the use of the NLH model within the Markov-Chain Monte-Carlo (MCMC) procedure. The latter was developed mainly for analyzing plasmas in the classical regime and hence the $\bar{Z} \sim 1.3$ merely played the role of a fitting parameter.

The result of the NPA calculations are in agreement with the conclusions of Ref. [10] that l-silicon at $\sim 4-5$ g/cm^3 is a good metal at 1 eV, with about a third of the conductivity of normal-density Al at the same temperature. Snap shots of of ionic positions in QMD simulations of l-Si are suggestive of complex transient bonding similar to that see in l-carbon. However, the long-time averaged (i.e., static) Si-Si pair distribution function of l-Si, calculated using the "one-atom"-DFT approach of the NPA agree well with that obtained from QMD calculations, as demonstrated in Sec. III, and in Sec. A4 of the Appendix detailing QMD simulations. These results should have implications regarding planetary magnetism due to the possibility of electrical currents in molten-Si cores.

In conclusion, the present analysis, using the all-electron DFT approach as employed in the NPA model, suggests that the WDM sample of l-Si created in the study by Poole et al [1] is very likely to be at a density of ~ 4.35 g/cm^3, at an ionization of four free electrons/ion, and in the pressure range 140-160 GPa. The NPA study presents a novel picture of l-silicon as a highly ionized metal showing a plethora of liquid-liquid phase transitions. Experimental pressure and temperature estimates may have significant uncertainties due to hysteresis effects, posing a further challenge to future experiments and theory.

VI. ACKNOWLEDGMENTS

The work of GG was partially supported by the United Kingdom EPSRC and First Light Fusion under the AMPLIFI Prosperity Partnership -EP/X025373/1. The first two authors (MWCD, DDK) have not received any specific funding for this work.

Appendix A

This appendix addresses the following topics.
(i) Brief description of the NPA calculations and the ion XC-functional.
(ii) Pseudopotential, Structure data and the first peak of $S(k)$.
(iii) Details of the QND calculations using VASP.
(iv) The short-ranged ionic structure across LPTs.
(v) Test of the non-linear Hulthén potential.
(vi) The compressibility ratio, electrical and thermal conductivities of l-Si.

1. Brief description of the NPA calculation

We do not consider well-defined ion configurations with ion-positions $R_1, R_2 \cdots, R_N$ in an N-ion simulation cell. Instead, the field ions are replaced by their smooth one-body distribution $\rho(r)$ since density functional theory (DFT) posits that the free energy is a functional of just the one-body density. Thus the N-body (multi-ion) problem is replaced by a one-body (i.e., one-ion) problem in the sense of DFT. This becomes exact if the ion correlation functional is exact. In practice it is approximate due to uncertainties in the XC-functionals. The electron density is also a smooth spherically symmetric distribution centered on the Si nucleus at the origin. We consider a sphere of radius $R_c \simeq 10r_{ws}$, i.e., a "correlation sphere" such that all correlation effects have died of an the densities $\rho(r), n(r)$ have reduced to their "bulk" average values $\bar{\rho}, \bar{n}$ respectively. The correlation sphere reduces to the Debye sphere in the classical low-density high-T limit. The central Si ion with its associated electron and ion distributions constitute a neutral object (the NPA) with bound and free electron states. The NPA can be applied with equal validity from the extreme quantum limit of high degeneracy at $T = 0$ to the non-degenerate classical limit, for fluids or solid phases [32].

Two coupled DFT variational equations appear in the theory of the NPA, since the total free energy $F([n], \rho]$ is a functional of two densities, viz, $n(r)$ and $\rho(r)$ [31].

$$\frac{\delta F}{\delta n} = 0, \;\; \frac{\delta F}{\delta \rho} = 0. \tag{A1}$$

The first of this equation can be analyzed and re-written as a Kohn-Sham equation for electrons subject to a one-body potential $V_e(r)$ inside the correlation sphere. The second equation can be treated using classical mechanics and reduces to a Boltzmann-like equation where the ions are subject to a one-body potential $V_I(r)$ that includes the nuclear potential, the Poisson potential and an ion XC-potential $V_{ii}^{xc}(r)$. There are small e-i XC-potentials that are neglected in this treatment [47, 48].

The Kohn-Sham calculation yields $n(r)$, as well as the Kohn-Sham eigenstates, eigen-energies and phase shifts of the "free-electron" states. As only a single ion center is used in NPA calculation, we do not have a highly inhomogeneous N-center electron distribution as in standard DFT simulations (e.g., using VASP [24]) where several hundred ions define a very complex electron distribution in a simulation cell. Instead, just a single-center spherical electron distribution $n(r)$ and an ion distribution $\rho(r)$ dependent on electron-electron and ion-ion correlation functionals occur in the NPA. This much smoother single-center electron density $n(r)$ can be conveniently treated using the local density approximation (LDA), as has been found from previous work. The electron exchange correlation functional used [49] in the LDA is a finite-T functional. Tests using other available functionals, e.g., the functionals by Karasiev et al [50], or by Groth et al [51] within the NPA code give essentially indistinguishable results for the range of densities and temperatures used in this study.

The XC-functional that reduces the multi-ion problem to a single-ion problem is known to be highly non-local and hence an LDA approximation is useless. However, as ions are classical particles, several simplifications arise. Although we use the generic name XC-potential, the exchange part in taken as zero and there is on a correlation functional to deal with. Furthermore, classical statistical mechanics and diagram techniques can be used to provide a numerically very convenient and accurate form for the ion-correlation functional $F_{ii}^{xc}[\rho(r)]$ if the irreducible "bridge" diagrams are neglected. When bridge diagrams are important (e.g., in high-density liquid Al near its melting point where hard-sphere-like packing effects are important), they can be included via the Lado-Foils-Ashcroft (LFA) approach [52]. However, we have shown ion previous work [10, 46] that bridge contributions are completely negligible in WDM systems like

C,Si where packing effects are not important. This because the ion-ion short-ranged structure is determined by electronic processes near the Fermi surface, and the associated long-ranged Friedel oscillations in the ion-ion pair potentials. The functional derivative of the XC-free energy with respect to the density is the corresponding ion-XC potential $V_{ii}^{xc}[\rho(r)]$. The latter is needed in the density functional equations. It can be given in the HNC-approximation as

$$\beta V_{ii}^{xc}(r) = -\bar{\rho}\int d\vec{r'}\left[h(\vec{r'}) + \beta V_I(\vec{r'})\right] h(|\vec{r}-\vec{r'}|) \quad \text{(A2)}$$

$$\beta V_I(r) = -\ln[g(r)], \;\; \beta = 1/T. \quad \text{(A3)}$$

This $V_{ii}^{xc}(r)$ is a highly non-local quantity, dependent on $h(r) = g(r) - 1$. In solving the coupled equations A1, the $g_{ii}(r)$ is initially approximated by a cavity $g(r)$ defined only by r_{ws} ; this r_{ws} is adjusted to self consistency via the two coupled DFT equations. Then the ion-ion pair- potential $V_{ii}(r)$, Eq. A6 is calculated via the pseudopotential, Eq. A3, generated from the final charge density $n(r)$. Then an HNC equation, or a modified HNC equation with bridge corrections [52] is solved to get a very accurate $g(r)$ instead of the initial cavity-$g(r)$ where only the cavity radius r_{ws} had been adjusted to be consistent with the final $\bar{Z}$ that satisfies the Friedel sumrule. This in effect provides a computationally convenient partial decoupling of the Kohn-Sham equation for electrons, and the corresponding classical DFT equation for ions [33].

The Kohn-Sham calculation provides bound states $\phi_{nl}(r)$ with energies ϵ_{nl} and continuum states $\phi_{kl}(r)$ with energies $\epsilon_{kl} = k^2/2$. These delocalized $\phi_{kl}(r)$ states behave asymptotically like plane waves with phase shifts δ_{kl}. They obey the finite-T Friedel sum rule [31], which determines the number of free electrons associated with each ion, namely $\bar{Z}$. So, at self-consistency, $\bar{Z} = \bar{n}/r\bar{h}o$ satisfies the Friedel sumrule, charge neutrality while being a key quantity in the thermodynamic equilibrium of the fluid, as it was evaluated via a minimization of the total free energy via Eq. A1. It has a clear physical meaning [31] and can be measured experimentally using Langmuir probes (for suitable plasma conditions). Indirect methods of determining $\bar{Z}$ are needed for WDM conditions.

The Kohn-Sham states of a Si-atom immersed in its ionic and electronic environment at $\rho = 4.6$ g/cm^3 and $T = 0.46$ eV are given in Table I. These results, as well as the Friedel sum evaluated from the Phase shifts unambiguously show that $\bar{Z} = 4$.

TABLE I. The electronic structure at a silicon nucleus in its fluid state for two cases. Case 1, $\bar{\rho} = 4.6$ g/cm^3 and T= 5300K($\simeq$ 0.46 eV). Case 2, $\bar{\rho} = 4.35$ g/cm^3 and T=1.2 eV. The energies are in Rydberg, while the mean orbital radius $< r_{nl} >$ is in atomic units. The Wigner-Seitz radii are is 2.537 a.u., and 2.585 a.u. for the two cases. Hence all bound states are seen to be compactly contained inside the Wigner-Seitz sphere. The Fermi momenta k_F and $t = T/E_F$ for the two cases are: 1.2007, 1.1786, and t=0.0235, 0.0635 respectively.

case	n, l	ϵ_{nl}	$< r_{nl} >$	occupation
1	1,0	-128.5	0.1120	1.0×2
2	1,0	-128.6	0.1120	1.0×2
1	2,0	-8.315	0.5738	1.0×2
2	2,0	-8.381	0.5733	1.0×2
1	2,1	-5.192	0.5416	1.0×6
2	2.1	-5.260	0.5407	1.0×6

2. Pseudopotential, Structure data and the first peak of $S(k)$

The Kohn-Sham-Mermin calculation described above, for a single ion of silicon immersed in its appropriate environment provides as with the bound density $n_b(r)$ from the bound wavefunctions, while the continuum wavefunctions provide a density $n_f(r)$ of free electrons, with $n_f(r) \to \bar{n}$ as $r \to R_c$. Hence the free-electron density pile up $\Delta n_f(r) = n_f(r) - \bar{n}$. We take this all-order result obtained from the Kohn-Sham calculation to be a result of a linear response to a weak electron-ion pseudopotential $U_{ei}(k)$, Then, if $\chi(k)$ is the full interacting electron response function at the density]$\bar{n}$ and temperature T, we have:

$$U_{ei}(k) = \Delta n_f(k)/\chi(k). \quad \text{(A4)}$$

Note that if a point ion of charge $\bar{Z}$ were considered, then its potential would be

$$U_{ei}^0(k) = -\bar{Z}V_k, \; V_k = 4\pi/k^2. \quad \text{(A5)}$$

. This point-ion interaction is a strong potential and cannot be used in linear-response theory. The weak pseudopotential that we use has a form factor W_k such that

$$W_k = U_{ei}(k)/U_{ei}^0(k). \quad \text{(A6)}$$

Since the finite-T response function of the uniform electron gas at finite-T inclusive its local-field correction can be constructed using the electron-electron XC-functional, $\chi(k)$ is a known quantity. Hence, the Kohn-Sham calculation can be processed to yield a weak electron-ion pseudopotential. The full details of the calculation may be found in Refs. [32, 33]. Furthermore, given the pseudopotential $U_{ei}(k)$, the corresponding pair-potential $V_{ii}(k)$ becomes

$$V_{ii}(k) = V_k\bar{Z}^2 + |U_{ei}(k)|^2\chi(k), \; V_k = 4\pi/k^2. \quad \text{(A7)}$$

This pair-potential can now be used in MD or in the hyper-netted-chain (HNC) equation to generate the structure factor ion-ion $S(k)$ and the corresponding PDF $g(r)$. In Ref. [35] it was shown that these pair potentials

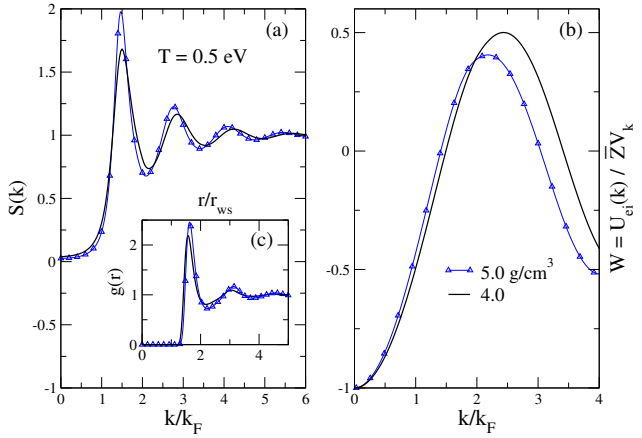

FIG. 7. (online color) Panel (a) of the figure shows the Si-Si $S(k)$ for $\bar{\rho}$=4.0 g/cm^3 and $\bar{\rho}$=5 g/cm^3 at T=0.5 eV. The position of the first peak of $S(k)$ in k-space (k_1) remains unchanged in spite of the variation in density by 25%, although the position of the first peak in r-space in $g(r)$ is affected. Panel (b) shows that the k_1 corresponds nearly to where the pair potential approximates to a strong point-ion interaction.

can be accurately fitted to a Yukawa-Friedel-Tail (YFT) form of the potential, viz:

$$V_{\rm yft}(r) = V_{\rm y}(r) + V_{\rm ft}(r), \quad \text{(A8)}$$

$$V_{\rm y} = (a_{\rm y}/r)\exp(-k_{\rm y}r), \quad \text{(A9)}$$

$$V_{\rm ft} = (a_{\rm ft}/r^3)\exp(-k_{\rm ft}r)\cos(q_{\rm ft}r + \phi_{\rm ft}). \quad \text{(A10)}$$

The Si-Si pair-potential taken in the form $V_{ii}(x)/T, x = r/r_{ws}$ at the density of 4.35 g/cm^3 ($r_{ws} = 2.5849$) and 1 eV can be fitted with the following values of the parameters. $a_{\rm y} = 1076.13, k_{\rm y} = 4.18038, a_{\rm ft} = 7.60699, k_{\rm ft} = 1.18818, q_{\rm ft} = 5.75909, \phi_{\rm ft} = 0.291775$.

In Fig. 7 we display the pseudopotential $U_{ei}(k)$, the structure factor $S(k)$ and $g(r)$ for liquid silicon at $T = 0.5$ eV, and at two densities, viz., 4.0 g/cm^3 and 5.0 g/cm^3. These the XRD and XRTS data of the experiment falls within these two densities. What is note-worthy is that the main peak of $S(k)$ has remained "pinned" at $k_1 \simeq 1.499$ which is in fact the value of k which makes the form factor W_k to be essentially zero. That is, the first peak of $S(k)$ tries to remain pinned to the value of k such that the pair-potential $V_{ii}(k)$ is strongest.

The relative stability of the short-ranged ionic structure over this density range is seen also in the g(r) shown in the inset to Fig. 6. we find that the short-ranged structure of the ions remains essentially unchanged over large changes of temperature and density, and even across LPTs.

3. Details of QMD calculations using VASP

The structure data (i.e., $g(r), S(k)$)obtained from the NPA have been established to be in good agreement in previous published work, for a variety of materials that include Al, Be, C, H, Li, Na, Si etc. In addition, in the present study also we have checked that our NPA calculations agree with results from QMD calculations for test cases. For instance, in Fig. 4 we display the results obtained for $g(r)$ for l-Si at 4.28-4.6 g/cm^3 at 1 eV using the Vienna Ab-initio simulation Package (VASP) [24].

The VASP simulations are for 64 atoms and carried out in a standard way [53], showing good agreement with the NPA results. An energy cutoff of $\sim$ 300 eV was employed. The (Monkhorst Pack) k-grid was used and calculations were done at the Γ point (0,0,0). Gaussian smearing (ISMEAR=0) with a smearing of 0.1 eV was imposed. The temperature was set using a Nosé-Hoover thermostat. The Purdew-Burke-Ernzerhof XC-functional [56] was used for electrons. It was ensured that the occupation in the highest energy state is less than 0.0001 even at the highest temperature studied.

In a previous QMD study [21] of l-Si and its PDFs, Remsing et al studied the convergence of PDFs and other selected properties for $N = 64$, 216, and 512, for the LDA, PBE and SCAN functionals. Best quantitative accuracy required the use of the SCAN functional and N=216, especially for obtaining good agreement with the melt line near 2.33 g/cm^3. Here we are considering l-Si at higher density and a higher temperature of 1 eV, favouring the use of smaller simulations. The $N = 64$ results, though somewhat noisy, were sufficiently well converged for our purpose of comparisons with the NPA. Increasing N of course gave better convergence to the NPA values. The larger N values, as well as the SCAN functional were needed in previous studies to capture the correlated phase of the liquid. In the present study (at the higher $\bar{\rho}, T$), the $N = 64$ calculations successfully recovered the correlated phase reported in Fig. 4(a) and (d). Due to our limited computational resources, only the $N = 64$-VASP simulations using the PBE functional are presented in this study, although some limited calculations weere done at $N = 125$.

4. The short-ranged ionic structure across LPTs

We noted in Sec. A 2 that it is energetically optimal to preserve the short-ranged ionic structure to position the electron-ion interactions at a zero of the pseudopotential. So, structural changes in the normal liquid occur in the long-ranged tails of the distribution functions, somewhat as in Martensitic transitions. These transitions appear as discontinuities in the compressibility and the pressure, while the short-ranged structure ($r/r_{ws} < 5$) remains more or less intact. This is demonstrated in Fig. 8 We see that the $g(r)$ and $S(k)$ remain unchanged when going from $\bar{\rho} = 4.28$ g/cm^3 to 4.32 g/cm^3 although the pressure and compressibility data show a discontinuity at 4.3 g/cm^3. Similar results are found for the other LPTs studied here. The LPTs seem to be similar to the well-known transition in l-Si at 2.5g/cm^3 near the melting point. However, we must note that the correlated liquid

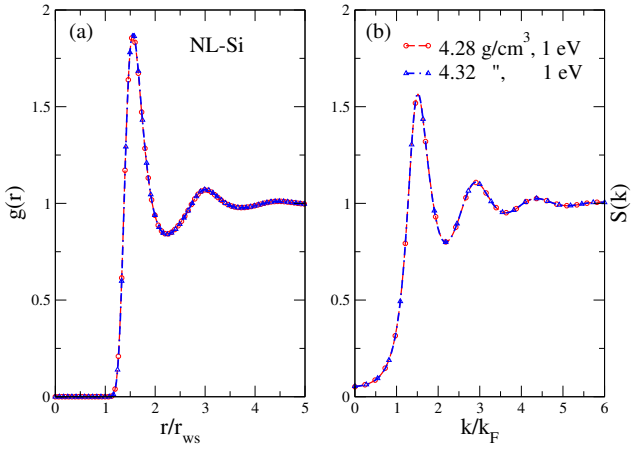

FIG. 8. (online color) Panel (a) The Si-Si $g(r)$) for $\bar{\rho}$=4.28 g/cm^3 and 4.32 g/cm^3 at T=1 eV, calculated using the NPA for the normal liquid phase. (b) The corresponding $S(k)$ are displayed.

(CL) phase has so far only been observed in numerical simulations, and not in experiments.

This insensitivity of the short-ranged structure to the LPTs makes them harder to detect via standard simulation methods. This is probably one reason why the much sought-after LPT in liquid carbon remained undetected until it was revealed via detailed NPA calculations [46].

5. Tests of the applicability of the Hulthén potential

The analysis of XRD and XRTS data given in Ref. [1] used the NLH potential as it is very simple to use, and has met with astrophysical applications in the past [27]. The first-principles potentials for silicon appropriate for a liquid-environment derived via the NPA can be used to test if the NLH potential is a satisfactory and simple substitute for use. Fig. 3 showed that NLH differed strongly from the DFT-based potentials calculated at 4.6 g/cm^3 and $T = 0.46$ eV.

As a further test, we used the QMD-generated $g(r)$ for l-silicon available for 2.5 g/cm^3, at T=1200K, and at $T = 1800$K where the SCAN functional has been used in the calculations [10, 21]. The QMD generated $g(r)$ agreed very closely with that from the NPA. We tried the NLH potential varying its $\bar{Z}$ to see if the QMD-$g(r)$ could be recovered, but this was not possible. This failure of the NLH-potential is a further reason justifying the present study.

6. The compressibility ratio, electrical and thermal conductivites of l-Si

The isothermal compressibility ratio ξ/ξ_0 and the electrical conductivity σ were displayed in Fig. 2 of the main text. Using ρ for the mean density $\bar{\rho}$ for simplicity, we use the equations given below.

$$\xi = \frac{1}{\rho}\left[\frac{\partial \rho}{\partial p}\right]_T = \xi_0\, S(0) \qquad \text{(A11)}$$

$$\xi_0 = 1/(\rho T), \text{ ideal gas.} \qquad \text{(A12)}$$

In Table II we give a tabulation of $\xi/\xi_0, \sigma$ together with the corresponding thermal conductivity κ calculated via the Lorentz number, using the approach given in Ref. [57]. As $\bar{Z}$= 4 for silicon, the Spitzer-Harm [58] analysis shows that e-e interactions can be neglected for high-$\bar{Z}$ values in calculating transport coefficients.

What is note worthy here is that while the density changes from $\sim$ 4 g/cm^3 to $\sim$ 5 g/cm^3, i.e., a change of

TABLE II. The isothermal compressibility ratio ξ/ξ_0 obtained from the $k \to 0$ limit of the ion-structure factor, the electrical conductivity σ calculated via the T-matrix [54, 55], and the thermal conductivity calculated via the Lorentz number [57] are tabulated below.

$T \to$		0.25 eV			1 eV	
$\bar{\rho}$ g/cm^3	ξ/ξ_0 $\times 0.1$	$\sigma \times 10^7$ [Sm]	$\kappa \times 10^2$ [Wm]	ξ/ξ_0 $\times 0.1$	$\sigma \times 10^7$ [Sm]	$\kappa \times 10^3$ [Wm]
4.20	0.1999	0.1064	0.7539	0.5390	0.1073	0.3043
4.22	0.1953	0.1063	0.7534	0.5338	0.1073	0.3044
4.24	0.1913	0.1062	0.7529	0.5278	0.1074	0.3045
4.26	0.1879	0.1061	0.7523	0.5226	0.1074	0.3047
4.28	0.2265	0.1059	0.7508	0.5168	0.1075	0.3048
4.30	0.2198	0.1058	0.7503	0.5126	0.1075	0.3049
4.32	0.2141	0.1057	0.7496	0.5454	0.1075	0.3050
4.34	0.2079	0.1056	0.7490	0.5404	0.1076	0.3050
4.36	0.2023	0.1056	0.7483	0.5351	0.1076	0.3051
4.38	0.1990	0.1055	0.7476	0.5302	0.1076	0.3052
4.40	0.1938	0.1054	0.7469	0.5249	0.1076	0.3052
4.42	0.1892	0.1053	0.7462	0.5199	0.1076	0.3053
4.43	0.1874	0.1052	0.7458	0.5175	0.1077	0.3053
4.44	0.1846	0.1052	0.7458	0.5140	0.1077	0.3053
4.46	0.1823	0.1050	0.7446	0.5101	0.1077	0.3053
4.48	0.1785	0.1049	0.7438	0.5049	0.1077	0.3053
4.50	0.1752	0.1048	0.7430	0.4989	0.1077	0.3053
4.52	0.1734	0.1047	0.7421	0.4946	0.1077	0.3053
4.54	0.1706	0.1046	0.7413	0.4889	0.1077	0.3053
4.46	0.1683	0.1045	0.7404	0.4835	0.1077	0.3053
4.48	0.1855	0.1044	0.7400	0.4782	0.1077	0.3053
4.60	0.1863	0.1043	0.7391	0.4744	0.1077	0.3053
4.62	0.1873	0.1041	0.7382	0.4692	0.1076	0.3052
4.64	0.1879	0.1034	0.7372	0.4732	0.1076	0.3052
4.66	0.1881	0.1038	0.7362	0.4705	0.1076	0.3051
4.68	0.1882	0.1037	0.7352	0.4694	0.1076	0.3051
4.70	0.1883	0.1036	0.7342	0.4666	0.1076	0.3059

25%, the electrical conductivity changes less than 3% at $T = 0.25$ eV, while at 1 eV, the change is less than 0.3%. The conductivity σ has been calculated using the phase-shifts of the continuum states via a T-matrix. However, we can understand the results more easily via the Ziman formula that uses a pseudopotential. The integrand $F(k)$ in the Ziman formula for the conductivity involves a product of $S(k)$ and the square of the pseudopotential $|U_{ei}(k)|^2$ in the neighbourhood of $k = 2k_F$. When the density changes, as seen from Fig. 7, $F(k)$ remains nearly invariant, with the changing density accommodated by small but collective changes in distant coordination shells. This happens in a cooperative manner leading to LPTs, as witnessed by the discontinuities in the pressure and the compressibility ratio.

[1] H Poole, M. K. Ginnane, M. Millot, H. M. Bellenbaum, G. W. Collins, S. X. Hu, D. Polsin, R. Saha, J. Topp-Mugglestone, T. G. White, D. A. Chapman, J. R. Rygg, S. P. Regan, and G. Gregori. Physical Review Research **6**, 023144 (2024) DOI: 10.1103/PhysRevResearch.6.023144

[2] A. Ng, T. Ao, F. Perrot, M.W.C. Dharma-wardana, M.E. Foord, Laser and particle beams, **23**, 527-537 (2005).

[3] E. E. McBride, A. Krygier, A. Ehnes, E. Galtier, M. Harmand, Z. Konôpková, *et al.,* Nature Phys. **15**, 89-94 (2019).

[4] L. I. Aptekar, Sov. Phys. Dokl. **24**, 993 (1979).

[5] I. Štich, R. Car, and M. Parrinello, Phys. Rev. Lett. **63**, 2240 (1989).

[6] M. W. C. Dharma-wardana and F. Perrot, Phys. Rev. Lett., **65**, 76 (1990).

[7] J. T. Okada, P. H.-L. Sit, Y. Watanabe, Y. J. Wang, B. Barbiellini, T. Ishikawa, *et al.,* Phys. Rev. Lett. **108**, 067402 (2012).

[8] M. W. C. Dharma-wardana, Contrib. Plasma Phys. **58** 128-142 (2018).

[9] S. X. Hu, R. Gao, Y. Ding, L. A. Collins, and J. D. Kress, Phys. Rev E **95**, 043210 (2017).

[10] M.W.C. Dharma-wardana, Dennis D. Klug, and Richard C. Remsing Phys. Rev. Lett. **125**, 075702 (2020). doi: 10.1103/PhysRevLett.125.075702

[11] S. Sastry and C. A. Angell, Nat. Mater. **2**, 739 (2003).

[12] S. S. Ashwin, U. V. Waghmare and Srikanth Sastry, Phys. Rev. Lett. **92**, 175701 (2004).

[13] T. Morishita, Phys. Rev. Lett. **93**, 055503 (2004)

[14] P. F. McMillan, M. Wilson, D. Daisenberger and D. Machon, Nat. Mater. **4**, 680 (2005).

[15] T. Morishita, Phys. Rev. Lett. **97**, 165502 (2006).

[16] P. Beaucage and N. Mousseau, J. Phys. Condens. Matter, **17**, 2269 (2005).

[17] Dominik Daisenberger, Mark Wilson, Paul F. McMillan, R. QuesadaCabrera, Martin C. Wilding, Denis Machon, Phys. Rev. B **75**, 224118 (2007).

[18] P. Ganesh and M. Widom, Phys. Rev. Lett. **102**, 075701 (2009).

[19] M. Baye, Martin Beye, Florian Sorgenfrei, William F. Schlotter, Wilfried Wurth, and Alexander Föhlisch, PNAS, **28**, 16772 (2010).

[20] V. V. Vasisht, S. Saw, and S. Sastry, Nat. Phys. **7**, 549 (2011).

[21] Richard C. Remsing, Michael L. Klein and Jianwei Sun, Phys. Rev. B **96**, 024203 (2017).

[22] Richard C. Remsing, Michael L. Klein and Jianwei Sun, Phys. Rev. B **97**, 140103(R) (2018).

[23] X.Gonze and C. Lee, Computer Phys. Commun. **180**, 2582-2615 (2009).

[24] G. Kresse and J. Furthmüller, Phys. Rev. B **54**, 11169 (1996).

[25] M. Schörner, M. Bethkenhagen, T. Döppner, D. Kraus, L. B. Fletcher, S. H. Glenzer, and R. Redmer, ing spectra from density functional theory molecular dynamics simulations based on a modified chihara formula, Phys. Rev. E **107**, 065207 (2023).

[26] B. B. L. Witte, M. Shihab, S. H. Glenzer, and R. Redmer, Phys. Rev. B **95**, 144105 (2017).

[27] Y. P. Varshni, Phys. Rev. A **41**, 4682 (1990).

[28] J. Vorberger, D. O. Gericke, and W.-D. Kraeft, High Energy Density Phys.**9**, 448 (2013).

[29] W.Ebeling, H. Reinholz, and G. Röpke, Eur. Phys. J.: Spec. Top. **229**,3403 (2020).

[30] E. M. Lifshitz and L. P. Pitaevaskii, *Physical Kinetics*, Pergamon, New York (1981), section 44.

[31] M. W. C. Dharma-wardana and F. Perrot, Phys. Rev. A **26**, 2096 (1982).

[32] F. Perrot, Phys. Rev. E **47**, 570 (1993).

[33] F. Perrot and M.W.C. Dharma-wardana, Phys. Rev. E. **52**, 5352 (1995).

[34] L. Dagens, J. Phys. C: Solid State Physics, **5**, 2333 (1972).

[35] M. W. C. Dharma-wardana, Lucas J. Stanek, and Michael S. Murillo Phys. Rev. E **106**, 065208 (2022).

[36] H. D. Whitley, D. M. Sanchez , S. Hamel , A. A. Correa, and L. X. Benedict, Contrib. Plasma Phys. **55**, 390 (2015).

[37] F. Ercolessi and J. B. Adams. EPL (Europhysics Letters), **26**(8), 583 (1994).

[38] P. Brommer, A. Kiselev, D. Schopf, P. Beck, J. Roth, and H.-R. Trebin. Modelling and Simulation in Materials Science and Engineering, **23**(7), 074002, (2015).

[39] Lucas J. Stanek, Raymond C. Clay III, M. W. C. Dharma-wardana, Mitchell A. Wood, Kristian R. C. Beckwith, and Michael S. Murillo, Phys. Plasmas **28**, 032706 (2021).

[40] D. Kraus, J. Vorberger, D. O. Gericke, V. Bagnoud, A. Blazevic, W. Cayzac, A. Frank, G. Gregori, A. Ortner, A. Otten, F. Roth, G. Schaumann, D. Schumacher, K. Siegenthaler, F. Wagner, K. Wunsch, and M. Roth, Phys. Rev. Let. **111**, 255501 (2013).

[41] J. Sun, B. Xiao, Y. Fang, *et al.* Phys. Rev. Lett. **111**, 106401 (2013).

[42] K. Kadau, T. C. Germann, P. S. Lomdahl, and B. L. Holian. Science, **296**, 1681 (2002) Shock waves.

[43] M. W. C. Dharma-wardana, Phys. Rev. E **86**, 036407 (2012).

[44] L. Harbour, M. W. C. Dharma-wardana, D. Klug and L. Lewis, Physical Review E **94**, 053211, (2016).

[45] W. Andreoni, Pys. Rev. B **14**, 4247 (1976).

[46] M. W. C. Dharma-wardana and Dennis D. Klug, Phys.

Plasmas **29**, 022108 (2022); doi: 10.1063/5.0077343
[47] F. Perrot, Y. Furutani and M.W.C. Dharma-wardana, Phys. Rev. A **41**, 1096-1104 (1990)
[48] E. K. U. Gross, and R. M. Dreizler, *Density Functional Theory*, NATO ASI series, **337**, 625 Plenum Press, New York (1993).
[49] F. Perrot and M. W. C. Dharma-wardana, Phys. Rev. B **62**, 16536 (2000); *Erratum:* **67**, 79901 (2003); arXive-1602.04734.
[50] Karasiev, V. V.; Sjostrom, T.; Dufty, J.; and Trickey, S. B.; *Phys. Rev. Lett.* **2014** *112* 076403.
[51] S. Groth, T. Dornheim, T. Sjostrom, F.D. Malone, W. Foulkes, M. Bonitz, Phys. Rev. Lett. **119** (13) 135001 (2017).
[52] F. Lado, S. M. Foiles and N. W. Ashcroft, Phys. Rev. **A 26**, 2374 (1983).
[53] Details for a standard MD simulation of l-Si using VASP are given in `https://www.vasp.at/wiki/index.php/Liquid_Si_-_Standard_MD`
[54] R. Evans, *Fundamentals of Inhomogeneous Fluids* (New York: Dekker) p 85 (1992).
[55] F. Perrot *et al.* and M. W. C. Dharma-wardana, Int. J. of Thermophys, **20**,1299 (1999).
[56] J. P. Perdew, K. Burke, and M. Ernzerhof, Phys. Rev. Lett. **77**, 3865 (1996).
[57] M. W. C. Dharma-wardana (unpublished) preprint: https://arxiv.org/abs/2404.19692
[58] L. Spitzer and R. Härm, Phys. Rev. **89**, 977 (1953).